Published OnlineFirst February 12, 2018; DOI: 10.1158/1535-7163.MCT-17-0377

Molecular Cancer Therapeutics

Impact of the Anticancer Drug NT157 on Tyrosine Kinase Signaling Networks

Shih-Ping Su[1,2], Efrat Flashner-Abramson[3], Shoshana Klein[3], Mor Gal[3], Rachel S. Lee[1,2], Jianmin Wu[4], Alexander Levitzki[3], and Roger J. Daly[1,2]

Abstract

The small-molecule drug NT157 has demonstrated promising efficacy in preclinical models of a number of different cancer types, reflecting activity against both cancer cells and the tumor microenvironment. Two known mechanisms of action are degradation of insulin receptor substrates (IRS)-1/2 and reduced Stat3 activation, although it is possible that others exist. To interrogate the effects of this drug on cell signaling pathways in an unbiased manner, we have undertaken mass spectrometry–based global tyrosine phosphorylation profiling of NT157-treated A375 melanoma cells. Bioinformatic analysis of the resulting dataset resolved 5 different clusters of tyrosine-phosphorylated peptides that differed in the directionality and timing of response to drug treatment over time. The receptor tyrosine kinase AXL exhibited a rapid decrease in phosphorylation in response to drug treatment, followed by proteasome-dependent degradation, identifying an additional potential target for NT157 action. However, NT157 treatment also resulted in increased activation of p38 MAPK α and γ, as well as the JNKs and specific Src family kinases. Importantly, cotreatment with the p38 MAPK inhibitor SB203580 attenuated the antiproliferative effect of NT157, while synergistic inhibition of cell proliferation was observed when NT157 was combined with a Src inhibitor. These findings provide novel insights into NT157 action on cancer cells and highlight how globally profiling the impact of a specific drug on cellular signaling networks can identify effective combination treatments. *Mol Cancer Ther; 17(5); 1–12. ©2018 AACR.*

Introduction

The past two decades have seen major advances in our understanding of the molecular mechanisms that underpin the different hallmarks of cancer, and these have led to the development of new classes of therapies that selectively target molecular mechanisms of specific importance to the survival and proliferation of cancer cells. However, the inherent genomic instability of cancer cells and their propensity to acquire additional mutations, coupled with intratumoral heterogeneity, means that the development of resistance to targeted therapies represents a major clinical problem (1). In light of this issue, the development of agents that can target several oncogenic signal transduction pathways, and/or factors in the tumor microenvironment that contribute to disease progression, has recently gained attention (2, 3).

The small-molecule drug NT157 represents a new class of anticancer agents that affect both the cancer cell and its supportive microenvironment (4–8). NT157 inhibits the proliferation of a wide variety of cancer cell lines *in vitro*, including those derived from colon, breast, and prostate cancer and melanoma, and reduces growth of melanoma and prostate cancer cell line xenografts as well as tumor burden in the CPC-APC mouse colon cancer model (6–8). It also inhibits metastasis of A375 melanoma xenografts (7). One mechanism of NT157 function is via degradation of insulin receptor substrate (IRS)-1/2 and hence inhibition of proproliferative and survival signaling mediated by these docking proteins. This mechanism involves direct allosteric modulation of the IGF-1R, uncoupling of the receptor from IRS-1/2, recruitment of Shc1, and activation of the Erk MAP kinases. The latter kinases then mediate serine phosphorylation of IRS1/2, leading to their degradation by the proteasome (7). However, NT157 also acts by reducing levels of activated, tyrosine-phosphorylated Stat3 via stimulation of an uncharacterized protein tyrosine phosphatase (4, 8). Stat3 plays a major role in the cross-talk between tumor cells and their microenvironment, and reflecting this, NT157 treatment of mouse melanoma and colon cancer models leads to reduced tumor inflammation, reactive stroma, and macrophage infiltration (4, 8). The ability of NT157 to inhibit two independent signaling pathways critical for cancer cell proliferation, survival, and metastasis, as well as cancer cell interaction with the tumor microenvironment, makes it a promising anticancer agent that may prove refractory to development of acquired drug resistance.

To date, interrogation of the mechanism of action of NT157 has been based on candidate-based approaches. However, application of global, unbiased strategies may reveal novel effects of this drug on cancer cell signaling pathways, thereby identifying additional potential NT157 targets as well as potential ways to improve NT157 efficacy. Because mass spectrometry (MS)–based

[1]Cancer Program, Biomedicine Discovery Institute, Monash University, Melbourne, Australia. [2]Department of Biochemistry and Molecular Biology, Monash University, Melbourne, Australia. [3]Department of Biological Chemistry, Unit of Cellular Signaling, The Alexander Silberman Institute of Life Sciences, The Hebrew University of Jerusalem, Jerusalem, Israel. [4]Key Laboratory of Carcinogenesis and Translational Research (Ministry of Education/Beijing), Centre for Cancer Bioinformatics, Peking University Cancer Hospital & Institute, Beijing, China.

Note: Supplementary data for this article are available at Molecular Cancer Therapeutics Online (http://mct.aacrjournals.org/).

Corresponding Author: Roger J. Daly, Department of Biochemistry and Molecular Biology, School of Biomedical Sciences, Level 1, Building 77, Monash University, Melbourne, Victoria 3800, Australia. Phone: 613-9902-9301; Fax: 613-9902-9500; E-mail: roger.daly@monash.edu

doi: 10.1158/1535-7163.MCT-17-0377

Published OnlineFirst February 12, 2018; DOI: 10.1158/1535-7163.MCT-17-0377

phosphoproteomic profiling represents a powerful strategy to resolve the impact of particular drugs on oncogenic signaling networks (9, 10), we have applied this approach to NT157. This reveals novel potential modes of action of NT157, including inhibition of AXL and activation of p38 MAPKs, as well as pathways that may limit drug efficacy and represent candidates for combination treatment.

Materials and Methods

Cell culture

Human A375 melanoma cells were obtained from the ATCC in 2008. The following human melanoma cell lines were also utilized: A375SM from the MDA Cancer Centre, Houston, TX in 2009; and M571 and M2068 provided by Dr. Michal Lotem at Hadassah Medical Center, Jerusalem, Israel, in 2012. A375 and M2068 cells were subject to additional validation in our laboratory by short tandem repeat polymorphism in March 2017. All cell lines were routinely checked for mycoplasma contamination by PCR and utilized for experiments within 4 passages. A375 cells were maintained in RPMI1640 medium supplemented with 10% FCS and 100 U/mL penicillin and 100 mg/mL streptomycin, and maintained at 37°C/5% CO_2. A375 SM cells were grown in MEM supplemented with 10% FBS, whereas M571 and M2068 cells were maintained in RPMI/DMEM/F12 in the ratio 1:3:1, supplemented with 10% FBS.

Small-molecule drugs

The molecular structure of NT157 is reported in Reuveni and colleagues (7). NT157 was synthesized in-house as described previously (7). The Src inhibitor PP1 and p38 MAPK inhibitor SB203580 were obtained from Synthos Ltd. and Calbiochem, respectively. Crizotinib and MG132 were purchased from Selleckchem and Sigma Aldrich, respectively.

Preparation of A375 cell lysates for phosphoproteomic profiling

Human melanoma A375 cells were seeded in 15-cm dishes for 24 hours. The medium was replaced with starvation medium (RPMI supplemented with antibiotics, without serum), and the cells were incubated overnight. The cells were then treated with NT157, 3 μmol/L, for 1 or 8 hours, or with vehicle (0.03% DMSO) for 8 hours. The cells were then washed twice with ice-cold PBS, then lysed in lysis buffer [8 mol/L urea, 20 mmol/L HEPES, 2.5 mmol/L sodium pyrophosphate, 2.5 mmol/L β-glycerophosphate, 1 mmol/L sodium orthovanadate, 1 mmol/L EDTA, 1 mmol/L tris (2-carboxyethyl) phosphine (TCEP)], and kept on ice for 20 minutes. Lysates were briefly sonicated then centrifuged (16,000 × *g*, 20 minutes, 4°C). Supernatants were collected and stored at −80°C. Two sets of biological replicate samples were prepared for all treatment conditions.

Phosphopeptide immunoprecipitation

Phosphopeptide immunoprecipitation was performed as described previously (11), with minor modifications. Proteins were reduced using 1 mmol/L TCEP and alkylated for 30 minutes with 4 mmol/L iodoacetamide at room temperature. The urea concentration in the cell lysates was diluted to 2 mol/L using 50 mmol/L ammonium bicarbonate, and cell lysates were digested with lysyl endopeptidase (1:200, w/w, Wako Laboratory Chemicals) for 4 hours at room temperature. The urea concentration was further diluted to 0.8 mol/L, and cell lysates were digested overnight using Sequencing Grade Modified Trypsin (1:100, w/w, Promega). Digested samples were desalted using Sep-Pak columns (Waters) as per the manufacturer's instructions. Two "spike-in" heavy peptides with alanine (al) C13N15 modifications were added prior to Sep-Pak clean-up (Sep-Pak, Waters). These peptides were EF1A1 (EHA(al)LLApYTLGVK) (500 fmol) and MAPK14 (HTDDEMTGpYVA(al) (10 pmol; Mimotopes). Phosphopeptides in the samples were enriched through sequential overnight immunoprecipitations using resin-bound P-Tyr-100 antibody (9411, Cell Signaling Technology), followed by P-Tyr-20 antibody (610000, BD Biosciences). p-Tyr antibodies were prebound to Protein G Sepharose resin (GE Healthcare Life Sciences) by incubating antibody and resin at a 1:4 ratio (w/v) overnight at 4°C. Phosphopeptides were eluted from the antibody–resin conjugate by adding 0.1 % trifluoroacetic acid, 40% acetonitrile, after 3 washes with IAP buffer [50 mmol/L Tris-HCl (pH 7.4), 150 mmol/L NaCl, 1% n-octyl-b-D-glucopyranoside, cOmplete EDTA-free Protease Inhibitor Cocktail Tablet (Roche)], and 4 washes with Milli-Q H_2O. Phosphopeptide samples were lyophilized by centrifugal evaporation, and resolubilized in 0.1% formic acid, 2% acetonitrile for LC/MS-MS analysis.

LC/MS-MS identification and quantitation

Enriched peptides were analyzed using a Q Exactive Plus Hybrid Quadrupole-Orbitrap Mass Spectrometer (Thermo Fisher Scientific) coupled to a Dionex UHPLC. Peptides were separated over a gradient of 65 minutes at a flow rate of 250 nL/minute. The scan range for MS1 analysis was 375 to 1,600 m/z, and the top 12 most intense ions were fragmented with higher energy collision-induced dissociation using a target value of 10,000 ions. The scan range for MS/MS analysis was 200 to 2,000 m/z.

MS data analysis

Raw MS data were analyzed using MaxQuant software version 1.5.2.8. Database searching was performed using the Andromeda search engine integrated into the MaxQuant environment against the human UniProt database release 2015_01, concatenated with known contaminants as well as the reversed sequences of all entries. The MaxQuant search included fix modifications of carbamidomethyl and variable modifications of oxidation, acetyl (Protein N-term) and phosphorylation (STY), and was limited to a maximum of two missed cleavages. From the MaxQuant search data, only phosphotyrosine sites with $P \geq 0.75$ were used for subsequent data analyses. The label-free intensity values for the EF1A1 and MK14 heavy peptides in each cell line were averaged and a subsequent normalization factor generated. Label-free MS intensity values for each pTyr site quantified in the dataset were divided by the appropriate normalization factor. Data from two biological replicates and both antibodies (P-Tyr-100 and P-Tyr-20) were combined and analysed together. Data from each phosphotyrosine site was normalized to the highest value across treatments, which was arbitrarily set as 1.

Bioinformatic analyses

Clustering of data was achieved using the Graphical Proteomics Data Explorer (GProX) program. KOBAS was used to perform pathway enrichment analysis (12). The hypergeometric test was selected to test statistical enrichment of KEGG and Reactome pathways, and the *P* values were corrected for multiple comparisons (13). The protein–protein interactions among proteins of interest were retrieved from the Protein Interaction Network Analysis platform (14), and substrate–kinase relationships were

Published OnlineFirst February 12, 2018; DOI: 10.1158/1535-7163.MCT-17-0377

Table 1. Effect of NT157 on *in vitro* activity of diverse protein kinases

Kinase	(ATP; μmol/L)	Compound IC_{50}* (mol/L): NT157 Data 1	Compound IC_{50}* (mol/L): NT157 Data 2	Control compound IC_{50}* (mol/L)	Control compound ID
AXL	100	5.53E−06	5.51E−06	1.36E−08	Staurosporine
BLK	10	9.19E−07	9.35E−07	1.59E−08	Staurosporine
c-MET	10	9.69E−06	9.63E−06	2.54E−07	Staurosporine
c-Src	15	3.71E−06	3.85E−06	3.94E−09	Staurosporine
EGFR	1	4.38E−06	3.99E−06	6.40E−08	Staurosporine
EPHA2	50	6.72E−06	6.79E−06	9.91E−08	Staurosporine
FGFR1	5	2.11E−06	2.05E−06	1.27E−09	Staurosporine
FGR	50	6.68E−06	7.05E−06	3.93E−09	Staurosporine
FLT1/VEGFR1	2.5	5.81E−06	6.42E−06	7.14E−09	Staurosporine
FRK/PTK5	30	3.55E−06	3.27E−06	7.75E−08	Staurosporine
FYN	30	5.32E−06	5.60E−06	6.01E−09	Staurosporine
HCK	30	2.80E−06	2.85E−06	4.32E−09	Staurosporine
IGF1R	30	3.25E−06	3.36E−06	1.22E−07	Staurosporine
JNK1	15			1.29E−06	Staurosporine
JNK2	20			4.81E−06	Staurosporine
JNK3	30			6.98E−07	JNKi VIII
LCK	15	1.01E−05	1.03E−05	1.84E−09	Staurosporine
LYN	15	5.10E−06	5.20E−06	1.77E−09	Staurosporine
P38a/MAPK14	2.5			4.26E−08	SB202190
P38b/MAPK11	50			2.39E−07	SB202190
P38d/MAPK13	30	1.42E−05	1.61E−05	7.36E−07	Staurosporine
P38g	50			1.69E−06	Staurosporine
PDGFRa	5	9.76E−06	8.95E−06	4.11E−10	Staurosporine
YES/YES1	50	4.67E−06	4.47E−06	4.79E−09	Staurosporine

NOTE: Compounds were tested in 10-dose IC_{50} mode in duplicate with 3-fold serial dilution starting at 10 μmol/L. Control compound staurosporine was tested in 10-dose IC_{50} mode with 4-fold serial dilution starting at 20 μmol/L. Alternate control compounds were tested in 10-dose IC_{50} mode with 3-fold serial dilution starting at 20 μmol/L. Reactions were carried out at Km ATP. Empty cells indicate no inhibition or compound activity that could not be fitted to an IC_{50} curve. IC_{50} value higher than 10 μmol/L is estimated on the basis of the best curve fitting available.

downloaded from the PhosphoSitePlus database (15). Cytoscape (16) was used for visualization of networks.

Western blot analysis

A375 cells were plated in 10-cm plates, and 24 hours later, the medium was replaced with starvation medium lacking FCS. Following 24-hour starvation, the cells were treated with NT157 (3 μmol/L) for 0.5 to 8 hours, or vehicle. The cells were harvested in hot Laemmli sample buffer and subjected to Western blot analysis as described previously (7). Antibodies used were as follows: from Cell Signaling Technology, pY702 AXL (#5724), AXL (#4566), pT180/Y182 p38 MAPK (#9211), JNK (#9258) YES1 (#3201), pY416 Src (#6943); R&D systems, pY779 AXL (# AF2228); Abcam, pY705 Stat3 (Ab76315), Stat3 (Ab50761); Santa Cruz Biotechnology, p38 MAPK (#535), pT183/Y185 JNK (#6254), GAPDH (#47724), β-actin (sc-69879); Sigma-Aldrich, α-tubulin (T5168).

Treatment of A375 cells with MG132 and NT157

A375 cells were seeded in 10-cm plates, and 24 hours later, the medium was replaced with starvation medium. Following 24-hour starvation, cells were pretreated with MG132 (10 μmol/L) for 1 hour before treatment with NT157 (3 μmol/L) or DMSO vehicle for 2 hours. Cells were harvested in hot Laemmli sample buffer and subjected to Western blot analysis using the indicated antibodies.

Knockdown of YES1 using siRNAs

A375 cells (0.6×10^6/well) were reverse transfected in 6-well plates using DharmaFECT 4 (2 μL per well) and a total concentration of 40 nmol/L of Dharmacon ON-TARGET plus SMARTpool siRNA targeting YES1 (L-003184-00-005) or the nontargeting (siOTP) control (D-001810-10). After 24 hours, the media were changed to complete medium. After another 24 hours, the medium was changed to starvation medium. Following 24 hours of starvation, the cells were treated with NT157 (3 μmol/L) or the DMSO vehicle for 2 hours before harvesting into hot Laemmli sample loading buffer and Western blot analysis.

Screen of NT157 activity against a kinase panel

This was undertaken by Reaction Biology Corp. For details, refer to Table 1 and Supplementary Table S2.

AXL *in vitro* kinase activity assay

The AXL *in vitro* kinase activity assay was performed using the AXL Kinase Enzyme System and ADP-Glo assay (Promega) following the manufacturer's instructions. Briefly, recombinant AXL kinase domain (50 ng) was incubated with the peptide substrate AXLtide (0.2 μg/μL) in the presence of 1 mmol/L ATP for 1 hour at room temperature before addition of the ADP-Glo reagent for a further 1 hour at room temperature. The kinase detection reagent was then added and incubated at room temperature for 30 minutes before luminescence was detected using the CLARIOstar microplate reader (BMG LABTECH).

Cell proliferation assays

A375 cells were plated in a 96-well plate (1,500 cells/well). Twenty-four hours later, the medium was replaced with fresh medium with vehicle control or specific drugs or drug combinations. Cell proliferation was assessed by methylene blue assay, 72 hours later.

Combination index

To calculate the combination index (CI), we used the formula $a/A + b/B$, where a is the dose of NT157 and b is the dose of PP1,

Published OnlineFirst February 12, 2018; DOI: 10.1158/1535-7163.MCT-17-0377

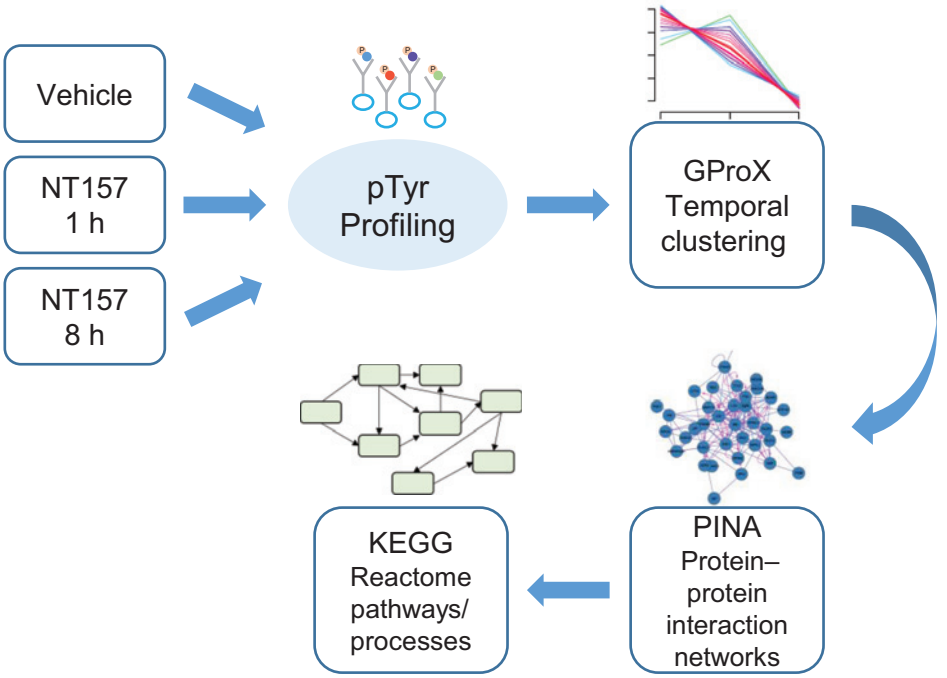

Figure 1.
Schematic of workflow. A375 melanoma cells were treated with vehicle or NT157 and cell lysates subjected to immunoaffinity-coupled LC/MS-MS. An integrated bioinformatic workflow was then utilized to resolve effects of NT157 on cell signaling networks over time. GProX was used to identify clusters of phosphotyrosine peptides related by virtue of similarity in their temporal response to drug treatment, PINA to characterize corresponding protein–protein interaction networks, and KEGG/ Reactome was used to identify cellular pathways and processes enriched within each cluster.

which, when combined, give the same effect as dose A of NT157 alone or dose B of PP1 alone. A CI < 1 indicated synergy.

RT-PCR

A375 cells were seeded into 6-well plates. After 24 hours, cells were washed twice with 1× PBS and placed in starvation medium for a further 24 hours. Cells were then treated with DMSO or 3 μmol/L NT157 for 2 hours. RNA was extracted using the RNeasy Mini Kit (Qiagen). RNA (1 μg) was converted to cDNA using a High-Capacity cDNA Reverse Transcription Kit (Applied Biosystems). Relative levels of *Axl* were determined by PCR using the following primers: sense 5′-AACCTTCAACTCCTGCCTTCTCG-3′ and antisense 5′-CAGCTTCTCCTTCAGCTCTTCAC-3′. Actin was used as the control with the following primers: sense 5′-GGCATCCTCACCCTGAAGTA-3′ and antisense 5′-GGGGTGTTGAAGGTCTCAAA-3′. The PCR amplification was performed using OneTaq Quickload 2× master mix with standard buffer (New England Biolabs) according to the manufacturer's instructions. PCR conditions were: initial denaturation at 94°C for 30 seconds, followed by 30 cycles of 94°C for 30 seconds, 55°C for 60 seconds and 68°C for 20 seconds, and a final extension at 68°C for 20 seconds. Amplified products were resolved on a 1.5% (w/v) agarose gel and visualized by staining with RedSafe (iNtRON Biotechnology). Densitometry was performed using ImageJ 1.48v (http://imagej.nih.gov/ij).

Results

Global phosphoproteomic profiling of NT157-treated cells

To determine the impact of NT157 on the tyrosine phosphoproteome, A375 cells were treated with either vehicle control or drug for 1 or 8 hours. Cell lysates were then subjected to immunoaffinity-coupled LC/MS-MS analysis (17) to qualitatively and quantitatively profile changes in tyrosine phosphorylation over the time course. This led to the identification of 193, 228, and 247 class I phosphotyrosine sites (high confidence localization probability of >0.75) from the vehicle control, 1-hour treatment, and 8-hour treatment sample, respectively (Supplementary Table S1). The data were then subjected to an integrated bioinformatic workflow to resolve effects of NT157 on cell signaling networks over time (Fig. 1). This analysis comprised three steps. First, GProX was used to identify clusters of phosphotyrosine peptides related by virtue of similarity in their temporal response to drug treatment. Second, the individual clusters were analyzed by PINA (14) to characterize corresponding protein–protein interaction networks. Third, interrogation by KEGG/Reactome was used to identify cellular pathways and processes enriched within each cluster. This approach led to the identification of 5 clusters of phosphotyrosine-containing peptides characterized by distinct temporal responses to NT157 treatment (Supplementary Table S1; Fig. 2).

Phosphotyrosine sites exhibiting decreased abundance

Although NT157 has been identified as an inhibitor of IRS and Stat3 signaling, it is unclear as to whether other signaling pathways are antagonized by this drug. Therefore, our analysis initially focused on proteins that exhibit rapid (within 1 hour) or more delayed (between 1 and 8 hours) reductions in tyrosine phosphorylation in response to NT157 (Clusters 2 and 4, respectively). A heatmap and protein–protein interaction network for Cluster 2 are shown in Fig. 3A and B. Although no cellular pathway or process was significantly enriched within this cluster, a striking result was a rapid decrease in phosphorylation of the receptor tyrosine kinase (RTK) AXL on Y702 within the activation loop, and accompanying reduction in phosphorylation of the nonRTK TNK2 on Y284 and Y859. Because TNK2 is a known downstream effector of AXL (18), the decreased phosphorylation of TNK2 is consistent with NT157 negatively regulating AXL signal output. A rapid decrease in phosphorylation of IRS-4 Y779 was also detected, although the known NT157 targets IRS-1, IRS-2, or Stat3 were not present within this Cluster. Bioinformatic analysis

Published OnlineFirst February 12, 2018; DOI: 10.1158/1535-7163.MCT-17-0377

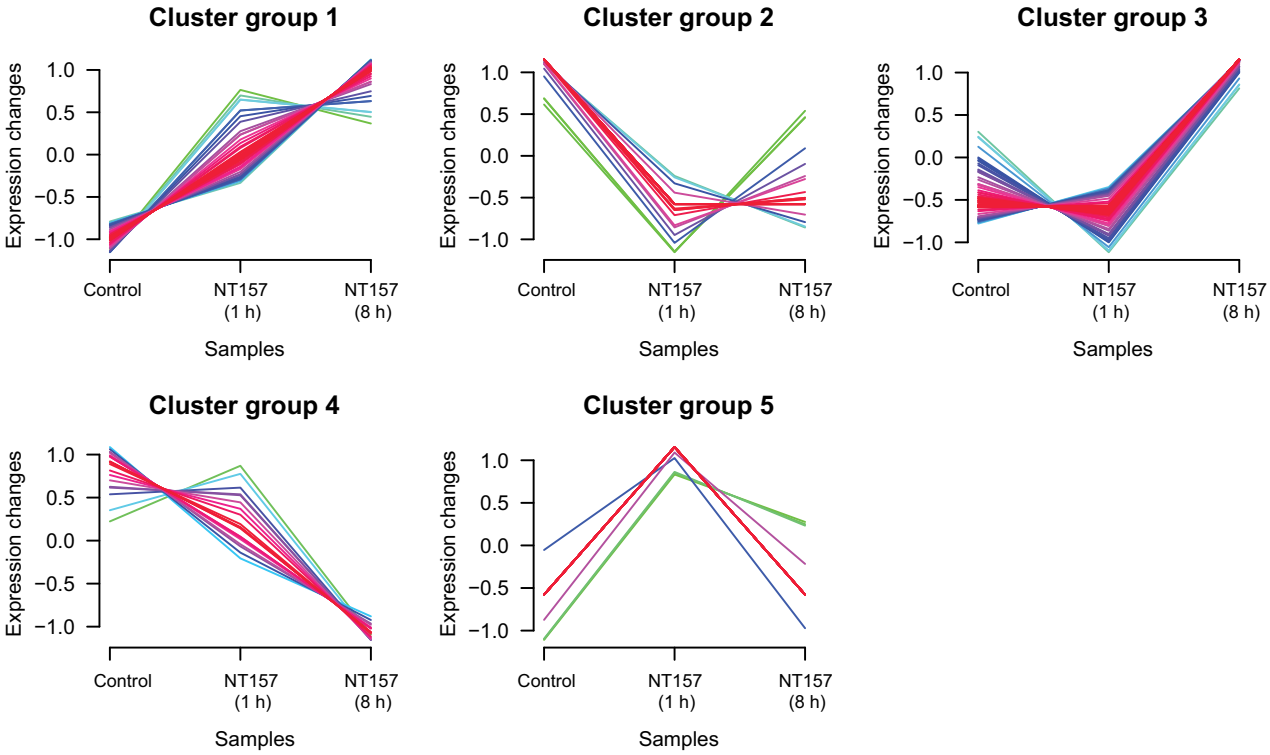

Figure 2.
GProX temporal clustering. The MS dataset was subjected to GProX temporal clustering, which resolved 5 clusters of phosphotyrosine-containing peptides characterized by distinct temporal responses to NT157 treatment.

of Cluster 4 (heatmap provided as Supplementary Fig. S1) revealed a protein–protein interaction network with PTK2 (also known as FAK) as a major hub, and significant enrichment for cell–cell communication and both VEGF and DCC signaling, reflecting decreased phosphorylation of proteins, such as spectrin alpha chain, VASP, PTK2 (on the key regulatory site Y397), SHB, DOCK1, and PIK3R2 (Fig. 4A and B).

Interestingly, the focal adhesion protein and PTK2 interactor NEDD9 (Fig. 4A) exhibited decreased phosphorylation on two sites in Cluster 2 (Fig. 3A) and also 2 sites within Cluster 4 (Supplementary Fig. S1), revealing that this focal adhesion scaffolding protein exhibits both rapid, and delayed, decreases in phosphorylation on specific sites. However, as noted in the following section, specific sites on NEDD9 also increase in phosphorylation following drug treatment, indicating that the impact of NT157 on this scaffolding protein is complex. ERBB3 and INSR were also members of the PTK2 interaction hub in Cluster 4 (Fig. 4A).

Of note, although a previous study used phosphospecific antibodies to demonstrate decreased abundance of Y896-phosphorylated IRS-1 and Y612-phosphorylated IRS-1/2 upon NT157 treatment, this was undertaken on IGF-1–stimulated cells. Because our study was performed on serum-starved cells without IGF-1 treatment, this may explain the absence of these sites from Clusters 2 and 4.

Phosphotyrosine sites exhibiting increased abundance

The allosteric mode of action of NT157 on the IGF-1R results in engagement of the receptor with Shc rather than IRS proteins, and enhanced Erk activation (7). Given this apparent "switch" in receptor signaling, it was of interest to determine whether other pathways are upregulated in response to this drug. Such enhanced signaling might also reflect relief of negative feedback mechanisms, as observed upon application of mTOR inhibitors (19). Consequently, identifying such pathways might not only provide insights into the mechanism of NT157 action, it may also identify potential strategies for improving the efficacy of this drug.

Protein–protein interaction and pathway analysis for sites exhibiting rapid increases in tyrosine phosphorylation (Cluster 1) are presented in Fig. 5A and B, with an accompanying heatmap shown as Supplementary Fig. S2. Cluster 1 corresponds to a dense protein–protein interaction network featuring numerous Src family kinases (SFK; SRC, LCK, LYN, FYN, YES1), RTKs (EGFR, EphA2, DDR2, INSR), several signaling proteins (PTPN11, PIK3R1, PLCG1), the focal adhesion proteins BCAR1 and NEDD9, and HSP90AB1 (Fig. 5A). In the case of the SFKs, it should be noted that the activation loop phosphopeptide detected is indistinguishable for SRC, LCK, FYN, and YES1. However, the corresponding peptide for LYN (corresponding to Y376) is nonidentical, so we can conclude from the MS analyses that LYN and at least one of the other 4 SFKs is exhibiting increased activation at 1 hour after drug treatment. Western blotting of lysates from control and NT157-treated A375 cells with a phospho-antibody selective for the activation loop of SFKs detected two bands of approximately 60 kDa (Supplementary Fig. S3A). The intensity of the upper band exhibited a biphasic increase in response to 0.5 to 2 hours of NT157 treatment, whereas the lower band exhibited a progressive increase over this timeframe. Knockdown using

Published OnlineFirst February 12, 2018; DOI: 10.1158/1535-7163.MCT-17-0377

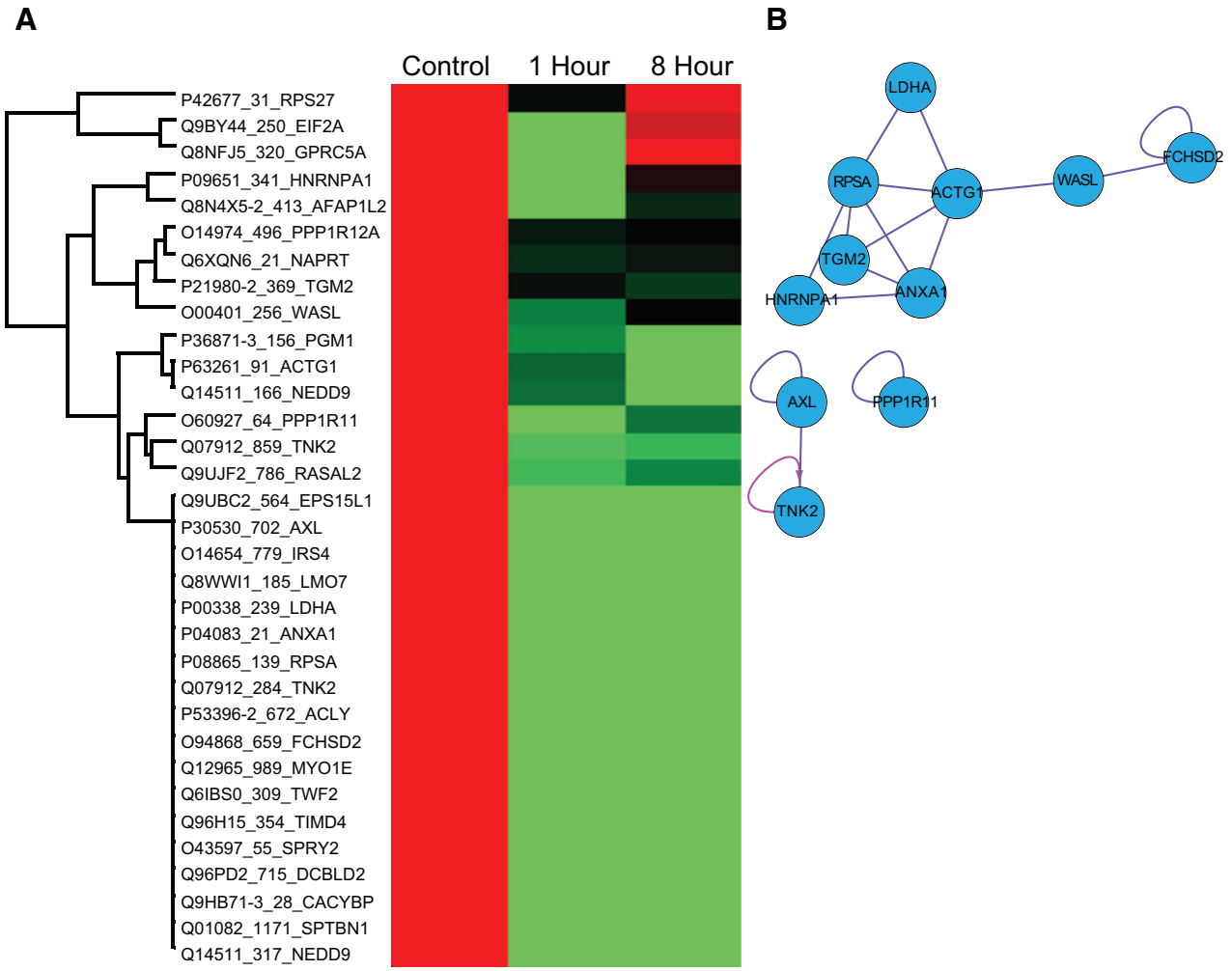

Figure 3.

Tyrosine phosphorylation sites exhibiting rapid reduction of phosphorylation in response to NT157 treatment. Heatmap (**A**) and protein–protein interaction network (**B**) for sites exhibiting rapid reductions (within 1 hour) in tyrosine phosphorylation (Cluster 2).

selective siRNAs determined that YES1 was a major contributor to the upper band, consistent with its slightly larger size compared with other SFKs, and a NT157-induced increase in intensity of this band was not observed following YES1 knockdown (Supplementary Fig. S3A and S3B). YES1 may also contribute to the lower band, either directly, or by promoting activation of other SFKs (Supplementary Fig. S3B). Although SRC, FYN, and LYN could be detected in A375 cells by Western blotting, knockdown of each SFK individually did not significantly affect the intensity of either band detected by the phospho-SFK antibody (Supplementary Fig. S3C). Consequently, either these kinases are not activated, or it is difficult to determine the contribution of each one individually by this approach. In the case of LYN, the latter explanation is more likely, as increased phosphorylation of the corresponding activation loop peptide could be detected by MS (Supplementary Table S1). LCK could not be detected in A375 cells.

The presence of PTPN11 in Cluster 1 may reflect the increased expression of this protein observed in certain cell lines following NT157 treatment (8). In addition, a striking result was increased activation of MAPK9 (JNK2), MAPK12 (p38 MAPK γ), and MAPK14 (p38 MAPK α) at this time point. The presence of numerous SFKs and signaling proteins are reflected in a significant enrichment for specific signaling pathways upon KEGG/Reactome searches (Fig. 5B). Interestingly, similar to Cluster 1, sites corresponding to specific RTKs (ERBB3, MET), signaling proteins (CRKL, PIK3R2, PLCG1), focal adhesion proteins (PTK2, BCAR1, NEDD9), and the stress-related kinases MAPK10/MAPK8 (JNK3/JNK1) were also present in Cluster 5 (rapid increase, then decrease; Supplementary Figs. S4 and S5A and S5B). However, this Cluster lacked the SFKs of Cluster 1.

The final cluster that we identified and interrogated, Cluster 3, exhibited a delayed induction upon NT157 treatment (Fig. 2; Supplementary Figs. S6 and S7A and S7B). Although this Cluster contained many proteins, a prominent aspect of the protein–protein interaction network was the presence of major "hubs" corresponding to HSP90AA1, HSP90AB1, and HSPA1A (Supplementary Fig. S7A), resulting in "cellular response to heat" being among the significantly enriched Reactome categories along with

Published OnlineFirst February 12, 2018; DOI: 10.1158/1535-7163.MCT-17-0377

A

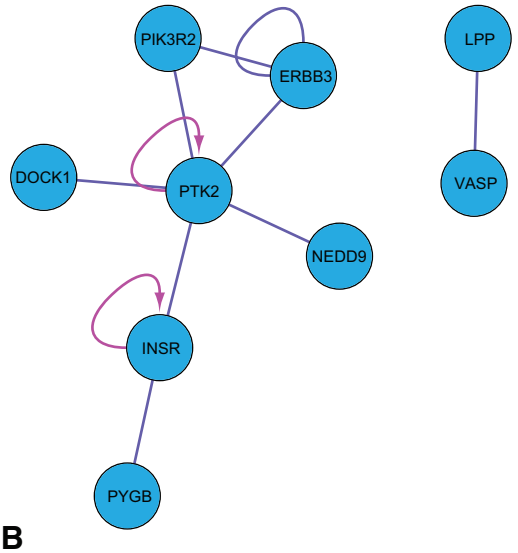

Figure 4.

Tyrosine phosphorylation sites exhibiting delayed reduction of phosphorylation in response to NT157 treatment. Protein–protein interaction (**A**) and pathway analysis (**B**) for sites exhibiting delayed reductions (by 8 hours) in tyrosine phosphorylation (Cluster 4).

B

Pathway	Database	Number of proteins	*P*	Corrected *P*	Genes
Cell–cell communication	Reactome	4	0.000273697	0.031064633	*Q13813|P50552|Q05397|O00459*
VEGFA–VEGFR2 Pathway	Reactome	4	0.000273697	0.031064633	*Q15464|Q14185|Q05397|O00459*
Signaling by VEGF	Reactome	4	0.000421283	0.031877108	*Q15464|Q14185|Q05397|O00459*
DCC-mediated attractive signaling	Reactome	2	0.000644042	0.036549361	*Q14185|Q05397*

examples corresponding to semaphorin, Eph, adhesion, and cytoskeletal signaling (Supplementary Fig. S7B). Also of note was that MAPK1 was present within this cluster, consistent with the previously reported stimulation of ERK activity by NT157 (7).

NT157 affects both AXL tyrosine phosphorylation and expression levels

Western blotting with appropriate site-selective phosphospecific antibodies confirmed that NT157 treatment leads to a rapid decrease in AXL Y702 phosphorylation (Fig. 6A). Interestingly, this preceded a later decrease in Y779 phosphorylation that reflected an overall reduction in AXL expression, first evident after 2 hours of NT157 treatment. Note that in Fig. 6A, the graphs indicate relative phosphorylation, so that the absolute level of active AXL was still markedly suppressed at 8 hours of treatment. Western blotting also validated the rapid induction of JNK and p38 MAPK activation in response to NT157. Because NT157 administration is known to result in reduced Stat3 activation (4, 8), blotting for Stat3 Y705 was included as a positive control in this experiment.

To further interrogate the mechanism of action of NT157 on AXL, we commissioned a screen that tested the effect of NT157 on the *in vitro* kinase activity of diverse protein kinases. The panel included AXL, representatives of other RTK subfamilies, different SFKs, the JNKs, and the p38 MAPKs (Supplementary Table S2). In this screen, which was undertaken at an ATP concentration corresponding to the Km for each kinase, NT157 exhibited an IC_{50} against AXL of approximately 5.5 μmol/L (Table 1). Although this indicates that NT157 can directly inhibit AXL kinase activity *in vitro*, and the IC_{50} is comparable with the concentration of NT157 used in our cell–based assay (3 μmol/L), we believe that direct inhibition is unlikely to explain the effects of NT157 on AXL tyrosine phosphorylation in cells, for several reasons. First, NT157 exhibited poor selectivity for AXL versus other kinases included in the screen. In this regard, the IC_{50} for AXL was comparable with the IC_{50}s for kinases that actually exhibited increased phosphorylation upon NT157 treatment of cells, such as EGFR and EphA2 (Table 1; Fig. 5A). Second, the Km ATP for AXL is 100 μmol/L, while the concentration of ATP in cells is approximately 1 mmol/L. If NT157 acts as an ATP-competitive kinase inhibitor, then the higher ATP concentration in cells will likely render NT157 inactive in cells at 3 μmol/L. Indeed, in an *in vitro* kinase assay undertaken in our laboratory at 1 mmol/L ATP, NT157 at 3 μmol/L did not significantly inhibit AXL activity, in contrast to crizotinib, which is known to represent an effective AXL inhibitor *in vitro* (Fig. 6B; ref. 20). Third, the IC_{50} for NT157 against AXL is much higher than that for previously characterized AXL-selective inhibitors. For example, the IC_{50} for R428 is approximately 0.01 μmol/L (21). Given these considerations, the effect of NT157 on AXL tyrosine phosphorylation in cells is unlikely to reflect direct inhibition of the kinase domain. The data from the kinase panel also indicate that the ability of NT157 to stimulate SFK, p38 MAPK, and JNK activity in cells must reflect indirect mechanisms, as either no effect of NT157, or inhibition by the drug, was observed in the corresponding *in vitro* assays (Table 1).

The ability of NT157 to reduce AXL protein expression levels could reflect transcriptional or posttranscriptional regulation. Determination of AXL mRNA levels by RT-PCR indicated that

Published OnlineFirst February 12, 2018; DOI: 10.1158/1535-7163.MCT-17-0377

A

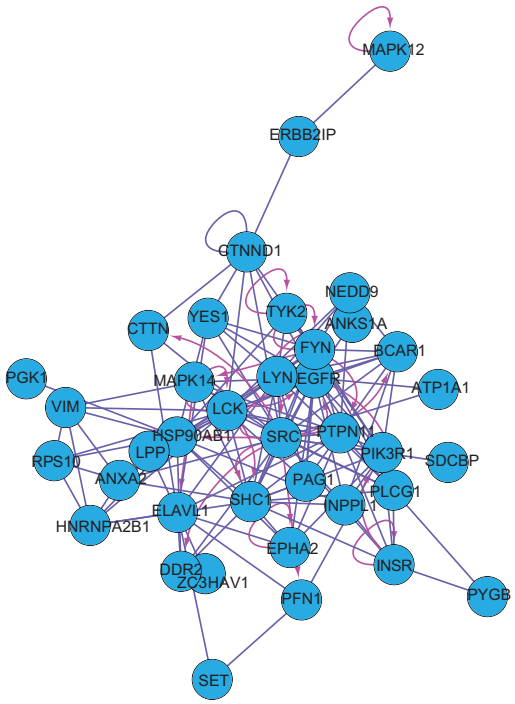

B

Pathway	Database	Number of proteins	*P*	Corrected *P*	Genes
PECAM1 interactions	Reactome	6	6.24E–09	2.68E–06	*P19174|Q06124|P07947|P06239|P06241|P07948*
IL3, 5, and GM-CSF signaling	Reactome	7	1.75E–06	0.000375	*P27986|P29353|Q06124|P07947|O15357|P06241|P07948*
CTLA4 inhibitory signaling	Reactome	5	6.59E–06	0.000709	*Q06124|P07947|P06241|P07948|P06239*
Signaling by ERBB2	Reactome	11	6.59E–06	0.000709	*P00533|P27986|P12931|P29353|Q96RT1|P19174|Q06124|P07947|P29597|P06239|P06241*
Cell surface interactions at the vascular wall	Reactome	8	1.36E–05	0.000984	*P27986|P29353|P19174|Q06124|P07947|P06239|P06241|*P07948
Signaling by interleukins	Reactome	9	1.37E–05	0.000984	*P27986|P29353|Q06124|P07947|P29597|O15357|P06239|P06241|P07948*
Signaling to ERKs	Reactome	6	1.93E–05	0.001052	*P53778|P29353|Q16539|P19174|Q06124|P29597*
VEGFA–VEGFR2 Pathway	Reactome	9	1.96E–05	0.001052	*P27986|P53778|Q16539|P19174|Q06124|P29597|P56945|O60716|P06241*
IL2 Signaling	Reactome	6	2.67E–05	0.001277	*P27986|P29353|Q06124|P29597|P06239|O15357*
Constitutive signaling by EGFRvIII	Reactome	4	4.01E–05	0.001508	*P29353|P00533|P27986|P19174*

Figure 5.
Tyrosine phosphorylation sites exhibiting rapid increases of phosphorylation in response to NT157 treatment. Protein–protein interaction (**A**) and pathway analysis (**B**) for sites exhibiting rapid increases in tyrosine phosphorylation (Cluster 1).

they were unchanged upon NT157 treatment (Fig. 6C), suggesting that NT157-induced alterations in AXL protein synthesis or stability might occur. To determine whether NT157 promotes AXL degradation, we pretreated cells with the proteasome inhibitor MG132. Although MG132 administration alone lowered AXL levels, consistent with a previous report (22), it prevented the NT157-induced reduction in AXL expression (Fig. 6D). These data indicate that in addition to reducing AXL tyrosine phosphorylation, NT157 promotes proteasome-dependent degradation of this RTK.

NT157 modulates AXL and SFK activation in multiple cell lines

To determine whether the NT157-mediated effects on cell signaling observed in A375 cells were broadly applicable, we utilized Western blot analysis to characterize how this drug impacted key pathways, including AXL expression and activation, in three additional melanoma lines (Fig. 7A). Although we could not detect AXL expression in the A375SM line (a metastatic derivative of A375; ref. 23), treatment with NT157 led to robust activation of SFKs and p38 MAPK, and inhibition of Stat3 phosphorylation, consistent with data from the parental line (Fig. 6A;

Published OnlineFirst February 12, 2018; DOI: 10.1158/1535-7163.MCT-17-0377

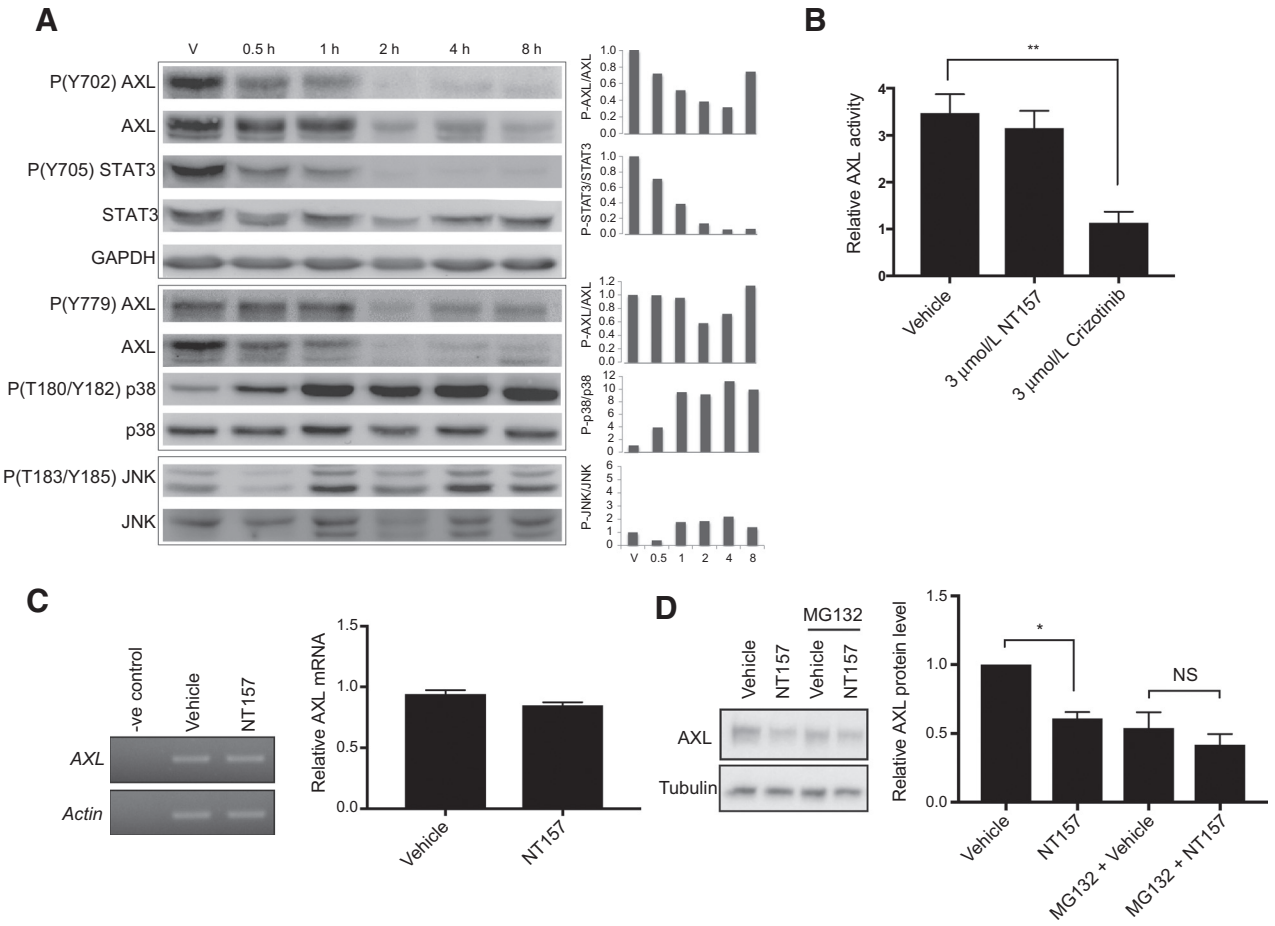

Figure 6.

Validation and further characterization of novel targets of NT157 action. **A,** Western blot analysis. A375 melanoma cells were treated with vehicle (V) or NT157 (3 μmol/L) for 0.5 to 8 hours, and then lysed. Cell lysates were Western blotted as indicated. The graphs on the right summarize densitometric analysis of the adjacent blots. **B,** Effect of NT157 on AXL *in vitro* kinase activity at a physiologic ATP concentration. The assay was undertaken as described in Materials and Methods at 1 mmol/L ATP. Data, mean and SEM, $n = 4$. **, $P < 0.01$ for crizotinib relative to vehicle control. **C,** Effect of NT157 on AXL mRNA levels. RT-PCR selective for AXL transcripts was undertaken on total RNA isolated from control and NT157-treated A375 cells 2 hours after drug treatment and analyzed by agarose gel electrophoresis. The histogram represents the mean and SEM from three independent experiments, with AXL expression normalized to that of actin. The negative control lacked template. **D,** Proteasome dependency of NT157-induced AXL degradation. A375 cells were either left untreated or preincubated for 1 hour with MG132 (10 μmol/L). Cells were then treated with NT157 (3 μmol/L) for 2 hours. Cell lysates were prepared and Western blotted as indicated. The histogram represents the mean and SEM from three independent experiments, with AXL expression normalized to the tubulin loading control. *, $P < 0.05$ for NT157 versus DMSO in the absence of MG132. NS, not significant.

Supplementary Fig. S3A). In M2068 melanoma cells, treatment with NT157 led to activation of Src (as determined from the ratio of pSrc/total Src) and p38 MAPK, decreased Stat3 phosphorylation, and NT157-induced reductions in AXL tyrosine phosphorylation and expression were also evident. In M571 melanoma cells, similar effects on AXL, Stat3, and p38 MAPK were detected, but an impact on SFKs was not observed. These data indicate that the novel effects of NT157 on AXL, SFKs, and p38 MAPK are not restricted to a single cell line.

Inhibition of p38 MAPK or SFKs has opposing effects on NT157 activity

Administration of NT157 to cells resulted in a marked activation of p38 MAPK (Figs. 5A and 6A). To determine how this pathway contributes to the antiproliferative effects of NT157, we cotreated cells with the selective p38 MAPK inhibitor SB203580 (24). The IC_{50} for inhibition of p38 MAPK by this drug is 0.3 to 0.5 μmol/L (25), and coadministration of SB203580 at 0.37 and 1.11 μmol/L markedly attenuated the antiproliferative effect of NT157, while monotreatment with SB203580 at these concentrations was without effect (Fig. 7B).

Because NT157 treatment also results in rapid SFK activation (Cluster 1, Fig. 5A), we characterized the effect of blocking SFK activity on the antiproliferative effects of NT157. Strikingly, when A375 melanoma cells were treated with NT157 and the small-molecule SFK-selective tyrosine kinase inhibitor PP1, alone or in combination, markedly enhanced inhibition of proliferation was observed for the combination treatment (Fig. 8). Extrapolating from the dose–response curves, approximately 11% inhibition of proliferation could be achieved by using 10 μmol/L PP1 or 0.29 μmol/L of NT157 in isolation, or a combination of 2.5 μmol/L PP1 and

Published OnlineFirst February 12, 2018; DOI: 10.1158/1535-7163.MCT-17-0377

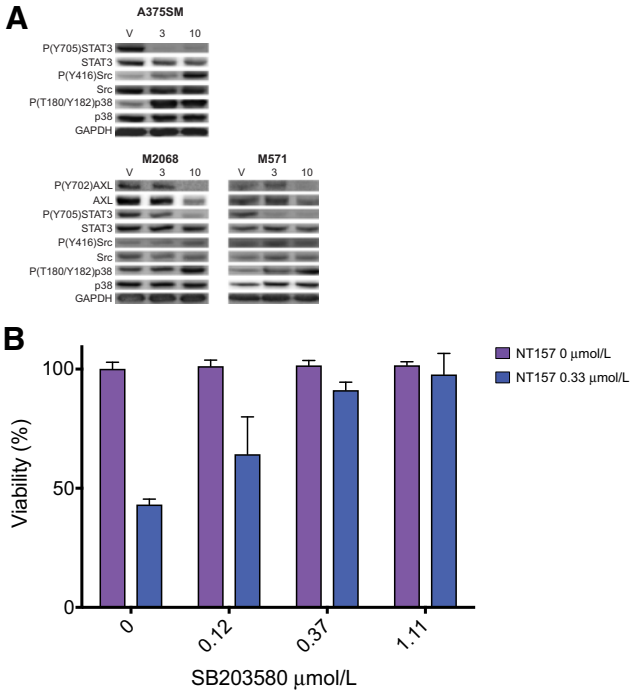

Figure 7.

Impact of NT157 on cell signaling pathways in different melanoma cell lines and effect of p38 MAPK inhibition on NT157 activity. **A,** Western blot analysis. Three different melanoma cell lines were treated with vehicle (V) or with NT157 at 3 or 10 μmol/L for 4 hours. Western blots were incubated with the indicated antibodies. Data shown are representative of three experiments. **B,** Effect of p38 MAPK inhibition on NT157 activity. A375 cells were treated with vehicle or NT157 (0.33 μmol/L) ± increasing concentrations of the p38 MAPK inhibitor SB203580. Cell proliferation was assayed methylene blue assay. Means and SEM of a representative experiment (out of three replicate experiments) are shown.

0.11 μmol/L NT157. Formal calculation of a CI using these values gives a value of 0.63, demonstrating synergy between the two drugs.

Overall, these data reveal that activation of p38 MAPK contributes to the antiproliferative effects of NT157 and also identify a novel strategy for enhancing the therapeutic efficacy of this drug. More broadly, they highlight how global characterization of signaling networks can identify important modes of action of novel drugs as well as nodes that mediate resistance and hence combination treatment modalities.

Discussion

The small-molecule drug NT157 has exhibited promising activity in preclinical studies (4, 6–8) as well as novel mechanisms of action that include allosteric modulation of the IGF-1R (7) and inhibition of Stat3 phosphorylation, with the latter effect apparently mediated via activation of an uncharacterized protein tyrosine phosphatase (4). In this study, we have utilized a global phosphoproteomic approach to determine that NT157 exerts complex effects on intracellular signaling networks, with resolution of 5 different clusters of tyrosine phosphorylation sites that differ in their directionality of response to drug treatment as well as temporal regulation. Despite this complexity, this approach has provided new insights into cellular effects of NT157 that highlight potential applications of this drug and strategies for development of more potent drug combinations.

An important finding was that NT157 inhibits activation loop phosphorylation of AXL within 1 hour of drug administration to cells. Given that AXL, and its downstream effector TNK2, were the only tyrosine kinases affected within this rapid inhibition cluster, this suggested that the decrease in AXL phosphorylation may be directly mediated by NT157. However, when tested for effects on *in vitro* kinase activity, NT157 exhibited poor selectivity toward AXL and was an ineffective inhibitor at a physiologic ATP concentration. Because these assays were undertaken with the kinase domain of AXL, one possibility is that NT157 binds to another region of AXL and represents an allosteric inhibitor. Alternatively, because NT157 promotes dephosphorylation of Stat3 (4), it may act via a related mechanism on AXL. Whatever the mechanism for this early effect on AXL tyrosine phosphorylation, NT157 then promotes degradation of this RTK, which occurs in a proteasome-dependent manner. Consequently, NT157 exerts a two-pronged attack on AXL signaling. Over the past decade, AXL has emerged as an important oncogenic kinase that is strongly implicated in the development and progression of several human cancers, including those of the breast, prostate and pancreas, non–small cell lung cancer (NSCLC), and acute myeloid leukemia (26). In addition, AXL mediates resistance to both conventional chemotherapy and specific targeted therapies, including EGFR inhibitors in NSCLC (26). Consequently, the identification of AXL as a likely NT157 target significantly expands the potential applications of this drug.

A key mechanism underpinning NT157 action is allosteric modulation of the IGF-1R, leading to uncoupling of the receptor from IRS1/2, recruitment of Shc1, and activation of the Ras/Raf/Erk cascade. This then leads to Erk-mediated serine/threonine phosphorylation of IRS1/2 and proteasomal degradation of these docking proteins (7). Interestingly, although activation of MAPK1 (ERK2) was detected in our study as a component of Cluster 3, we also determined that NT157 treatment leads to rapid activation of additional MAPK cascades, specifically p38 MAPKs α and γ, and JNK1–3. This is important for several reasons. First, the activation of these kinases may provide an additional pathway for serine/threonine phosphorylation of IRS proteins, as the JNKs in particular are known to phosphorylate and negatively regulate IRS-1 (27). Second, these stress-induced kinases may contribute to the proapoptotic effect of NT157 observed in certain cellular systems

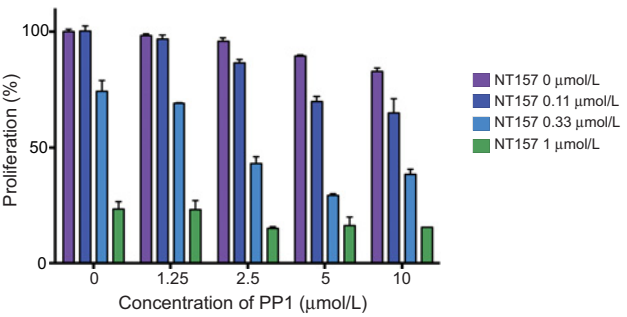

Figure 8.

Synergistic interaction of NT157 and Src inhibitor PP1. Cell proliferation was assayed as in Fig. 7B. Means and SEM of a representative experiment (out of four replicate experiments) are shown. Two-way ANOVA demonstrated a significant effect of combining PP1 and NT157 ($P < 0.0001$), and calculation of the CI confirmed synergy between the two drugs (see text).

Published OnlineFirst February 12, 2018; DOI: 10.1158/1535-7163.MCT-17-0377

(6, 28). Indeed, we determined that activation of p38 MAPK is required for the inhibitory effect of NT157 on cell proliferation. Third, because p38 MAPK and the JNKs are not classically downstream of Shc1/Ras, this supports the concept that NT157 has additional mechanisms of action beyond its known effect on the IGF-1R. A potential stimulus for these pathways is the increased phosphorylation of BCAR1 and NEDD9 detected in response to NT157, as these two related scaffolds are known to promote p38 MAPK and/or JNK activation (29, 30). Alternatively, NT157 may trigger their activation through stress-related mechanisms, although evidence for this is currently lacking.

A surprising result was the increased abundance of phosphorylated peptides corresponding to the activation loop of SFKs in response to drug treatment, which occurred as a rapid response to NT157 (Cluster 1). This may reflect IGF-1R inhibition by NT157, as a similar effect on SFKs occurs in rhabdomyosarcoma cells in response to anti–IGF-1R agents. Furthermore, as in our study, YES1 was a major contributor to this SFK response (31). The rapid NT157-induced activation of SFKs observed may explain the enhanced phosphorylation of known SFK substrates, such as BCAR1, NEDD9, HSP90AA1, and HSP90AB1 (Clusters 1, 3, and 5; refs. 32, 33). Because SFKs generate proliferative and prosurvival signals, we hypothesized that their increased activation may act to dampen the anticancer activity of NT157. Indeed, cotreatment of cancer cells with NT157 and the Src tyrosine kinase inhibitor PP1 resulted in synergistic inhibition of proliferation compared with either agent alone. Therefore, this identifies a novel strategy for enhancing the therapeutic efficacy of not only NT157, but also SFK inhibitors, which have demonstrated disappointing results in clinical trials evaluating activity against solid tumors (34). Developing this concept further, because the HSP90-associated chaperone complex is required for optimal activity of a variety of oncogenes and HSP90 cycling is positively regulated by tyrosine phosphorylation (35), combined treatment with NT157 and HSP90 inhibitors may also be effective.

In summary, this study has provided important mechanistic insights into the mechanism of action of NT157 and highlighted the power of the global phosphoproteomic approach to identify signaling network responses that limit therapeutic efficacy and that can be exploited for improved cancer cell targeting.

Disclosure of Potential Conflicts of Interest

No potential conflicts of interest were disclosed.

Authors' Contributions

Conception and design: E. Flashner-Abramson, A. Levitzki, R.J. Daly
Development of methodology: S.-P. Su, S. Klein, R.J. Daly
Acquisition of data (provided animals, acquired and managed patients, provided facilities, etc.): S.-P. Su, E. Flashner-Abramson, S. Klein, M. Gal, R.S. Lee
Analysis and interpretation of data (e.g., statistical analysis, biostatistics, computational analysis): S.-P. Su, S. Klein, R.S. Lee, J. Wu, R.J. Daly
Writing, review, and/or revision of the manuscript: S.-P. Su, E. Flashner-Abramson, S. Klein, R.S. Lee, J. Wu, R.J. Daly
Administrative, technical, or material support (i.e., reporting or organizing data, constructing databases): M. Gal
Study supervision: R.J. Daly

Acknowledgments

R.J. Daly is an NHMRC Principal Research Fellow (APP1058540).

The costs of publication of this article were defrayed in part by the payment of page charges. This article must therefore be hereby marked *advertisement* in accordance with 18 U.S.C. Section 1734 solely to indicate this fact.

Received April 27, 2017; revised October 11, 2017; accepted January 17, 2018; published first February 12, 2018.

References

1. Khamisipour G, Jadidi-Niaragh F, Jahromi AS, Zandi K, Hojjat-Farsangi M. Mechanisms of tumor cell resistance to the current targeted-therapy agents. Tumour Biol 2016;37:10021–39.
2. Martin M, Wei H, Lu T. Targeting microenvironment in cancer therapeutics. Oncotarget 2016;7:52575–83.
3. Zanardi E, Bregni G, de Braud F, Di Cosimo S. Better together: targeted combination therapies in breast cancer. Semin Oncol 2015;42:887–95.
4. Flashner-Abramson E, Klein S, Mullin G, Shoshan E, Song R, Shir A, et al. Targeting melanoma with NT157 by blocking Stat3 and IGF1R signaling. Oncogene 2016;35:2675–80.
5. Garofalo C, Capristo M, Mancarella C, Reunevi H, Picci P, Scotlandi K. Preclinical effectiveness of selective inhibitor of IRS-1/2 NT157 in osteosarcoma cell lines. Front Endocrinol 2015;6:74.
6. Ibuki N, Ghaffari M, Reuveni H, Pandey M, Fazli L, Azuma H, et al. The tyrphostin NT157 suppresses insulin receptor substrates and augments therapeutic response of prostate cancer. Mol Cancer Ther 2014;13:2827–39.
7. Reuveni H, Flashner-Abramson E, Steiner L, Makedonski K, Song R, Shir A, et al. Therapeutic destruction of insulin receptor substrates for cancer treatment. Cancer Res 2013;73:4383–94.
8. Sanchez-Lopez E, Flashner-Abramson E, Shalapour S, Zhong Z, Taniguchi K, Levitzki A, et al. Targeting colorectal cancer via its microenvironment by inhibiting IGF-1 receptor-insulin receptor substrate and STAT3 signaling. Oncogene 2016;35:2634–44.
9. Guo A, Villen J, Kornhauser J, Lee KA, Stokes MP, Rikova K, et al. Signaling networks assembled by oncogenic EGFR and c-Met. Proc Natl Acad Sci U S A 2008;105:692–7.
10. van der Mijn JC, Broxterman HJ, Knol JC, Piersma SR, De Haas RR, Dekker H, et al. Sunitinib activates Axl signaling in renal cell cancer. Int J Cancer 2016;138:3002–10.
11. Rikova K, Guo A, Zeng Q, Possemato A, Yu J, Haack H, et al. Global survey of phosphotyrosine signaling identifies oncogenic kinases in lung cancer. Cell 2007;131:1190–203.
12. Xie C, Mao X, Huang J, Ding Y, Wu J, Dong S, et al. KOBAS 2.0: a web server for annotation and identification of enriched pathways and diseases. Nucleic Acids Res 2011;39:W316–22.
13. Benjamini Y, Hochberg Y. Controlling the false discovery rate: a practical and powerful approach to multiple testing. J R Stat Soc Series B Methodol 1995;57:289–300.
14. Cowley MJ, Pinese M, Kassahn KS, Waddell N, Pearson JV, Grimmond SM, et al. PINA v2.0: mining interactome modules. Nucleic Acids Res 2012;40:D862–5.
15. Hornbeck PV, Kornhauser JM, Tkachev S, Zhang B, Skrzypek E, Murray B, et al. PhosphoSitePlus: a comprehensive resource for investigating the structure and function of experimentally determined post-translational modifications in man and mouse. Nucleic Acids Res 2012;40:D261–70.
16. Smoot ME, Ono K, Ruscheinski J, Wang PL, Ideker T. Cytoscape 2.8: new features for data integration and network visualization. Bioinformatics 2011;27:431–2.
17. Ali NA, Wu J, Hochgrafe F, Chan H, Nair R, Ye S, et al. Profiling the tyrosine phosphoproteome of different mouse mammary tumour models reveals distinct, model-specific signalling networks and conserved oncogenic pathways. Breast Cancer Res 2014;16:437.

Published OnlineFirst February 12, 2018; DOI: 10.1158/1535-7163.MCT-17-0377

18. Pao-Chun L, Chan PM, Chan W, Manser E. Cytoplasmic ACK1 interaction with multiple receptor tyrosine kinases is mediated by Grb2: an analysis of ACK1 effects on Axl signaling. J Biol Chem 2009;284:34954–63.
19. Sun SY, Rosenberg LM, Wang X, Zhou Z, Yue P, Fu H, et al. Activation of Akt and eIF4E survival pathways by rapamycin-mediated mammalian target of rapamycin inhibition. Cancer Res 2005;65:7052–8.
20. Cui JJ, Tran-Dube M, Shen H, Nambu M, Kung PP, Pairish M, et al. Structure based drug design of crizotinib (PF-02341066), a potent and selective dual inhibitor of mesenchymal-epithelial transition factor (c-MET) kinase and anaplastic lymphoma kinase (ALK). J Med Chem 2011;54:6342–63.
21. Holland SJ, Pan A, Franci C, Hu Y, Chang B, Li W, et al. R428, a selective small molecule inhibitor of Axl kinase, blocks tumor spread and prolongs survival in models of metastatic breast cancer. Cancer Res 2010; 70:1544–54.
22. Bae SY, Hong JY, Lee HJ, Park HJ, Lee SK. Targeting the degradation of AXL receptor tyrosine kinase to overcome resistance in gefitinib-resistant non-small cell lung cancer. Oncotarget 2015;6:10146–60.
23. Li L, Price JE, Fan D, Zhang RD, Bucana CD, Fidler IJ. Correlation of growth capacity of human tumor cells in hard agarose with their in vivo proliferative capacity at specific metastatic sites. J Natl Cancer Inst 1989;81: 1406–12.
24. Cuenda A, Rouse J, Doza YN, Meier R, Cohen P, Gallagher TF, et al. SB 203580 is a specific inhibitor of a MAP kinase homologue which is stimulated by cellular stresses and interleukin-1. FEBS Lett 1995;364: 229–33.
25. Lali FV, Hunt AE, Turner SJ, Foxwell BM. The pyridinyl imidazole inhibitor SB203580 blocks phosphoinositide-dependent protein kinase activity, protein kinase B phosphorylation, and retinoblastoma hyperphosphorylation in interleukin-2-stimulated T cells independently of p38 mitogen-activated protein kinase. J Biol Chem 2000;275:7395–402.
26. Wu X, Liu X, Koul S, Lee CY, Zhang Z, Halmos B. AXL kinase as a novel target for cancer therapy. Oncotarget 2014;5:9546–63.
27. Brummer T, Schmitz-Peiffer C, Daly RJ. Docking proteins. FEBS J 2010; 277:4356–69.
28. Wagner EF, Nebreda AR. Signal integration by JNK and p38 MAPK pathways in cancer development. Nat Rev Cancer 2009;9:537–49.
29. Barrett A, Pellet-Many C, Zachary IC, Evans IM, Frankel P. p130Cas: a key signalling node in health and disease. Cell Signal 2013;25:766–77.
30. Fashena SJ, Einarson MB, O'Neill GM, Patriotis C, Golemis EA. Dissection of HEF1-dependent functions in motility and transcriptional regulation. J Cell Sci 2002;115:99–111.
31. Wan X, Yeung C, Heske C, Mendoza A, Helman LJ. IGF-1R inhibition activates a YES/SFK bypass resistance pathway: rational basis for co-targeting IGF-1R and Yes/SFK kinase in rhabdomyosarcoma. Neoplasia 2015;17:358–66.
32. Barabutis N, Handa V, Dimitropoulou C, Rafikov R, Snead C, Kumar S, et al. LPS induces pp60c-src-mediated tyrosine phosphorylation of Hsp90 in lung vascular endothelial cells and mouse lung. Am J Physiol Lung Cell Mol Physiol 2013;304:L883–93.
33. Lee BY, Timpson P, Horvath LG, Daly RJ. FAK signaling in human cancer as a target for therapeutics. Pharmacol Ther 2015;146:132–49.
34. Creedon H, Brunton VG. Src kinase inhibitors: promising cancer therapeutics? Crit Rev Oncog 2012;17:145–59.
35. Xu W, Mollapour M, Prodromou C, Wang S, Scroggins BT, Palchick Z, et al. Dynamic tyrosine phosphorylation modulates cycling of the HSP90-P50 (CDC37)-AHA1 chaperone machine. Mol Cell 2012;47:434–43.

AACR American Association for Cancer Research

Molecular Cancer Therapeutics

Impact of the Anticancer Drug NT157 on Tyrosine Kinase Signaling Networks

Shih-Ping Su, Efrat Flashner-Abramson, Shoshana Klein, et al.

Mol Cancer Ther Published OnlineFirst February 12, 2018.